THE JOURNAL OF BIOLOGICAL CHEMISTRY
Vol. 277, No. 52, Issue of December 27, pp. 50573–50578, 2002
Printed in U.S.A.


# Crystal Structure of Venus, a Yellow Fluorescent Protein with Improved Maturation and Reduced Environmental Sensitivity*

Received for publication, September 17, 2002
Published, JBC Papers in Press, October 4, 2002, DOI 10.1074/jbc.M209524200

**Agata Rekas‡§, Jean-René Alattia‡¶, Takeharu Nagai‖**, Atsushi Miyawaki**, and Mitsuhiko Ikura‡ ‡‡**

*From the ‡Division of Molecular and Structural Biology, Ontario Cancer Institute and Department of Medical Biophysics, University of Toronto, Toronto, Ontario M5G 2M9, Canada, ‖Structure and Function of Biomolecules, PRESTO, JST, Nittochi 535 Akinono-cho Nakagyo-ku, Kyoto 604-0847, Japan, and the **Laboratory for Cell Function and Dynamics, Advanced Technology Development Center, Brain Science Institute, RIKEN, Wako-city, Saitama 351-0198, Japan*

**Yellow emission variants of green fluorescent protein (GFP) have been found useful in a variety of applications in biological systems due to their red-shifted emission spectrum and sensitivity to environmental parameters, such as pH and ionic strength. However, slow maturation properties and new requirements for more intense fluorescence necessitated further mutagenesis studies of these proteins. Venus, a new variant with improved maturation and brightness, as well as reduced environmental dependence, was recently developed by introducing five mutations into the well characterized variant, enhanced yellow fluorescent protein (EYFP). In this paper, we present the crystal structure of Venus at 2.2 Å resolution, which enabled us to correlate its novel features with these mutation points. The rearrangement of several side chains near the chromophore, initiated by the F46L mutation, was found to improve maturation at 37 °C by removing steric and energetic constraints, which may hinder folding of the polypeptide chain, and by accelerating the oxidation of the Cα–Cβ bond of Tyr$^{66}$ during chromophore formation. M153T, V163A, and S175G were also found to improve the rate of maturation by creating regions of greater flexibility. F64L induced large conformational changes in the molecule, leading to the removal of halide sensitivity by preventing ion access to the binding site.**

Green fluorescent protein (GFP),[1] originally isolated from the jellyfish *Aequorea victoria*, has been the subject of continued interest since its gene was first cloned in 1992 (1). The high stability of mature GFP over various environment conditions, the spontaneous autocatalytical generation of the fluorophore of GFP, and the possibility of spectral manipulation by mutagenesis, make GFP and its related proteins attractive tools for numerous biological applications (2).

Maturation of GFP proceeds in three major steps, beginning as the 238-residue single GFP polypeptide folds into its nearly native conformation. Residues 65–67 of the folded protein then undergo several chemical reactions necessary for chromophore formation, including cyclization and dehydration (3). The final rate-limiting step in the maturation process involves the oxidation of the Cα–Cβ bond of Tyr$^{66}$ by aerial oxygen. This maturation process takes ~3 h at room temperature and its efficiency further decreases at 37 °C, hindering the use of GFP in some biological applications. To improve maturation and performance at 37 °C, mutations such as F99S, M153T, and V163A have been introduced, creating valuable GFP variants for a wider range of applications (4, 5).

Thorough understanding of the relationship between the protein sequence and its physico-chemical properties requires three-dimensional structure determination of GFP at atomic resolution. Crystal structures of both the monomeric and dimeric forms of GFP have been solved previously (6, 7). The wild-type GFP (wtGFP) chromophore, which exists in equilibrium between two ground states, produces two maxima in the light absorption spectrum. The near-UV absorption peak at 395 nm originates from the neutral chromophore, while the ionic chromophore absorbs at a longer wavelength and produces a smaller peak at 475 nm (3). Green light is emitted from wtGFP at 503 nm. Spectral properties of GFP were shown to be influenced by its dimerization state (8), which is characterized by a dissociation constant of ~100 μM (9).

In the case of YFP, a yellow variant of GFP, the main absorption maximum of 514 nm corresponds to the chromophore ionic form and is red-shifted relative to wtGFP. Unlike wtGFP, the neutral form does not emit fluorescence efficiently, and the higher energy peak is largely suppressed (10). The equilibrium between the neutral and ionic forms of the YFP chromophore can be shifted in favor of the latter form by the following two mutations: S65G, which prevents hydrogen bond formation between residues Gly$^{65}$ and Glu$^{222}$, and T203Y, which produces additional polarizability around the chromophore. Also, the π-π interaction between Tyr$^{203}$ and the chromophore phenol ring reduces the excited state energy, thereby increasing the excitation and emission wavelengths (6).

When compared with the green emission variants of GFP, the absorbance level of YFP and its derivatives display a strong environmental sensitivity. The ratio between the two absorbance peaks, and therefore fluorescence efficiency, are dependent upon pH and the halide ion concentration (10, 11). This sensitivity makes YFPs efficient pH and halide sensors (12, 13), but for applications requiring stable fluorescence in a wide range of environment conditions, it is necessary to have proteins that are insensitive to pH and halides. Griesbeck and colleagues (14) developed a less sensitive variant of yellow

* This work was supported in part by the grant from Howard Hughes Medical Institute under the International Research Scholar program (to M. I.). The costs of publication of this article were defrayed in part by the payment of page charges. This article must therefore be hereby marked "*advertisement*" in accordance with 18 U.S.C. Section 1734 solely to indicate this fact.

§ Current address: Dept. of Chemistry, University of Wollongong, NSW 2522, Australia.

¶ Supported by the Caven postdoctoral fellowship.

‡‡ Canadian Institutes of Health Research Investigator. To whom correspondence should be addressed. Fax: 416-946-2055 (or 6529); E-mail: mikura@uhnres.utoronto.ca.

[1] The abbreviations used are: GFP, green fluorescent protein; wt, wild-type; YFP, yellow fluorescent protein; EYFP, enhanced YFP.

TABLE I
*Comparison of Venus, EYFP, and wtGFP*
Differences in sequence, $pK_a$, dissociation constant for chloride, and folding rate.

| | Residue | | | | | | | | | | $pK_a$[a] | $K_{fold}$[b] | $K_{d,Cl}$ |
|---|---|---|---|---|---|---|---|---|---|---|---|---|---|
| | 46 | 64 | 65 | 68 | 72 | 80 | 153 | 163 | 175 | 203 | | $s^{-1}$ | |
| Venus | CTG Leu | CTG Leu | GGC Gly | CTG Leu | GCC Ala | CAG Gln | ACC Thr | GCC Ala | GGC Gly | TAC Tyr | 5.8 | $5.62 \times 10^{-2}$ | $>10^4$ |
| EYFP | TTC Phe | TTC Phe | GGC Gly | CTG Leu | GCC Ala | CGC Arg | ATG Met | GTG Val | AGC Ser | TAC Tyr | 6.9 | $3.87 \times 10^{-3}$ | 2.53 |
| wtGFP | TTT Phe | TTC Phe | TCT Ser | GTT Val | TCA Ser | CAG Gln | ATG Met | GTG Val | AGC Ser | ACC Thr | 6.2 | $2.45 \times 10^{-2}$ | $>10^4$ |

[a] $pK_a$ for EGFP, EYFP, and Venus measured at 30 mM Cl; 150 mM ionic strength, and 25 °C.
[b] S65T (24).

fluorescent protein, citrine, which contained a Q69M mutation in addition to the four mutations used to create the original yellow variant EYFP(S65G/V68L/S72A/T203Y). This mutation helped decrease the pH and halide sensitivity and facilitated expression at 37 °C. With a relatively low value of $pK_a = 5.7$, citrine is particularly applicable in systems of lower pH and in a wide range of $Cl^-$ concentration.

More recently, Nagai *et al.* (15) introduced a new variant of yellow emission protein, called Venus, with reduced pH and halide dependence and an improved maturation rate. These properties were achieved in Venus by various mutations, which differ from those used in citrine (14). Instead of Q69M mutation used in citrine, Venus contains five other mutations (F46L, F64L, M153T, V163A, and S175G) in addition to the previously described four mutations characteristic to EYFP. The F46L mutation helps accelerate the oxidation step in chromophore formation, an effect which is specific to yellow emission proteins. The remaining four mutations are known to improve folding at 37 °C, and at least one was found to remove proton and chloride sensitivity (15) (Table I). The aim of our work was to solve the three-dimensional structure of Venus, shedding light on the structural basis of the observed molecular properties. We compared this crystal structure of Venus at 2.2-Å resolution with previously published structures of wtGFP (7) and EYFP (10) to pinpoint mutation-dependent structural changes. Our ultimate goal is to use systematic structural analysis of GFP mutants to provide future guidelines for rational design of improved variants.

## EXPERIMENTAL PROCEDURES

*Protein Expression and Purification*—Venus was subcloned into a $pRSET_b$ plasmid and expressed in the *Escherichia coli* strain $BL21(DE3)_{gold}$. Cells were grown using standard culture medium (LB broth) in a shaker incubator at 37 °C until the optical density of 0.7 was reached. Upon induction with isopropyl-1-thio-β-D-galactopyranoside, the temperature was lowered to 25 °C, and protein was expressed for 7–8 h. Protein containing the N-terminal polyhistidine tag was purified using nickel affinity chromatography. Subsequently, ion exchange and gel filtration were employed to achieve satisfactory levels of purity. The N-terminal $His_6$ tag was cleaved using enterokinase.

*Structure Determination*—The protein solution was concentrated to 33 mg/ml in 20 mM Tris hydrochloride (pH 7.9), with 50 mM NaCl and 0.5 mM dithiothreitol. Yellow fluorescent rod-shaped crystals ($P3_112$), with approximate dimensions of 0.5 × 0.08 × 0.08 mm, were grown in hanging drops containing 2 μl of protein and 2 μl of mother liquor at room temperature for 3–7 days. The mother liquor contained 2.1 M ammonium sulfate, 100 mM Tris hydrochloride at a pH of 8.4 and 4% (v/v) polyethylene glycol 400. The crystals were cryo-protected in 20% glycerol and 5% (v/v) polyethylene glycol 400, then flash-cooled to 100 K in a stream of $N_2$ gas. Diffraction data from a single crystal were collected in-house on a Mar345 imaging plate detector using Rigaku RU200 rotating anode as a generator of CuKα x-rays. 0.5 degree oscillations were collected in 300-s exposures. Data were collected to 97.7% completeness at 2.2-Å resolution. Unit cell dimensions were: $a = 82.704$, $b = 82.704$, $c = 72.555$ Å. The EYFP coordinate file (10), which served as a search model for phasing by molecular replacement, was edited by removing mutated residues and the chromophore to minimize bias. The parameters for the anionic chromophore were obtained from the Hetero-compound Information Centre, Uppsala, Sweden (HIC-up). Rigid-body refinement was carried out using the CNS program (16). Electron density maps ($2F_o - F_c$ and $F_o - F_c$) were inspected using the program O (17), and water molecules were added using CNS. Nine rounds of refinement interspersed with manual building in O, including introduction of water and polyethylene glycol molecules, resulted in $R_{cryst} = 22\%$ and $R_{free} = 25\%$. The data collection and refinement statistics are summarized in Table II. The following Protein Data Bank codes were used for structural comparison: 1GFL, dimeric wtGFP (7); 1YFP, EYFP (10); 1F09, H148Q EYFP with bound iodide (18); 1EMA, S65T GFP (6); and 1G7K, DsRed (19).

## RESULTS AND DISCUSSION

### *Chromophore Environment and Spectral Properties*

Venus was crystallized as a dimer with one molecule per asymmetric unit. The refined structure of Venus shows an 11-strand (labeled A to K from the N terminus) β-barrel, typical of GFP-derived fluorescent proteins. Calculated for α-carbons of residues 5–60 and 70–225, the root mean square deviation of a single Venus β-barrel relative to wtGFP and EYFP β-barrels is 0.32 and 0.35 Å, respectively. In all three structures compared, the cross-section taken perpendicularly to the long axis of the barrel is not perfectly circular but rather oval in shape. While the longer diameter of the oval cross-section of all three proteins is identical (23.8 Å; measured from distances of four Cα pairs), the shorter diameter differs between EYFP (22.3 Å) and Venus (21.9 Å). The difference in the oval shape between these yellow variants is closely related to the packing of interior amino acid residues and influences the integrity of dimer interface, as discussed below.

The residues surrounding the Venus chromophore are similar to those surrounding the chromophore of EYFP (Fig. 1*A*). More specifically, there are no significant changes between Venus and EYFP in the distances between the chromophore and residues $Thr^{62}$, $Leu^{68}$, $Gln^{69}$, $Gln^{94}$, $Arg^{96}$, $Asn^{146}$, $Arg^{168}$, $Gln^{183}$, $Tyr^{203}$, and $Ser^{205}$. Electron density studies of Venus show an 11° angle between the planes of the chromophore and $Tyr^{203}$, while the same angle measured in EYFP is 11.5–12.3°, making the plane of the Venus chromophore slightly more parallel than that of EYFP. This small difference may account for a minor change in the absorption spectrum of Venus relative to EYFP, as seen at a pH range of 4.6–8.6 and a 50 mM NaCl concentration. Although the position of the main absorption maximum remains unchanged (516 nm) in both Venus and EYFP, a smaller peak resulting from the neutral (protonated) chromophore is shifted in Venus by 20 nm producing a peak at 413 nm *versus* 393 nm in EYFP. The slightly more parallel orientation of the aromatic rings of $Tyr^{66}$ and $Tyr^{203}$ might also help improve the π-π interaction, thus reducing the excited state energy of the neutral chromophore. If this is the case, we can hypothesize that at lower pH, which is favorable to chromophore protonation, the angle between the rings would be smaller than 11°.

TABLE II
*Crystallographic statistics of Venus*

Numbers in parentheses refer to the highest resolution shell, 2.28–2.37 Å.

| | |
|---|---|
| Data collection | |
| Resolution (Å) | 2.2 |
| Total observations | 121,451 |
| Completeness (%) | 97.7 at 2.2 Å |
| $R_{merge}$ (%) | 7.6 (31.7) |
| Refinement statistics | |
| Space group | $P3_112$ |
| Molecules per asymmetric unit | 1 |
| $R_{cryst}$ | 0.218 |
| $R_{free}$ | 0.248 |
| Protein atoms | 1826 |
| Solvent atoms per asymmetric unit | 72 |
| Average B factor (Å$^2$) | 29.4 |
| Bond length deviations (Å) | 0.0006 |
| Bond angle deviations (°) | 1.376 |

One of the changes observed around the Venus chromophore is a 0.3-Å increase in the distance between the C$\alpha$–C$\beta$ bond and the OE1 atom of the Glu$^{222}$ side chain, compared with EYFP. A result of this increased distance is a 0.5-Å shift of the chromophore away from the protein surface and the Glu$^{222}$ side chain. Following this shift, an increased rate of oxidation is observed, attributed to enhanced oxygen access to the oxidation site in Venus. Other factors facilitating this reaction will be discussed under "Venus-specific Mutations."

Another difference in the Venus chromophore area, when compared with that of EYFP, is the presence of a shorter hydrogen bond (by 0.2 Å) between the chromophore phenolate and His$^{148}$. This may result from a slight rotation in the His$^{148}$ imidazole, making it less parallel to the $\beta$-barrel surface. However, this effect may also be due to the higher pH at which the crystals were grown (pH 8.5 for Venus, pH 6.9 for EYFP). The previously observed pH effect on S65T suggests that at a lower pH this distance becomes larger and hydrogen bonds are broken, consistent with our observations of Venus as well as past studies of EYFP (20).

The mutual position of the two chromophores within the Venus dimer differs from that of wtGFP and EYFP. The chromophore-chromophore distance in the Venus dimer is shorter than that of others by approximately 2 Å when measured using the phenol oxygens (Fig. 3*A*). These differences may be attributed mainly to the different orientation of subunits in the dimeric structure, coupled with the overall closer intersubunit contact in Venus than in EYFP (Fig. 2 and Table III).

### *Dimer Structure and Halide Sensitivity*

The subunit orientations in the Venus dimer (Fig. 1, *B* and *C*) are similar to those in the wtGFP dimer, but differ from those of EYFP. When the backbone chain of one Venus subunit is superimposed on that of wtGFP, the second subunits display a similar orientation with respect to the superimposed subunits. In contrast, following superimposition of the first subunit of Venus on that of EYFP, the second subunits display a significantly different orientation (Fig. 2*A*). The root mean square deviation for the aforementioned second subunits is 1.15 Å between Venus and wtGFP and 4.97 Å between Venus and EYFP. By using the angular parameters described in Table III, we can quantitatively define the unique orientation of the two subunits within the dimeric fluorescent proteins. The "tilt" angle between two subunits of Venus is similar to that of wtGFP, but differs from that of EYFP (Table III). These differences and similarities in domain orientations, depicted in Fig. 2*A*, clearly show the differences in the position of one subunit when the other subunit is superimposed.

Comparison of the buried surface areas for wtGFP, EYFP,

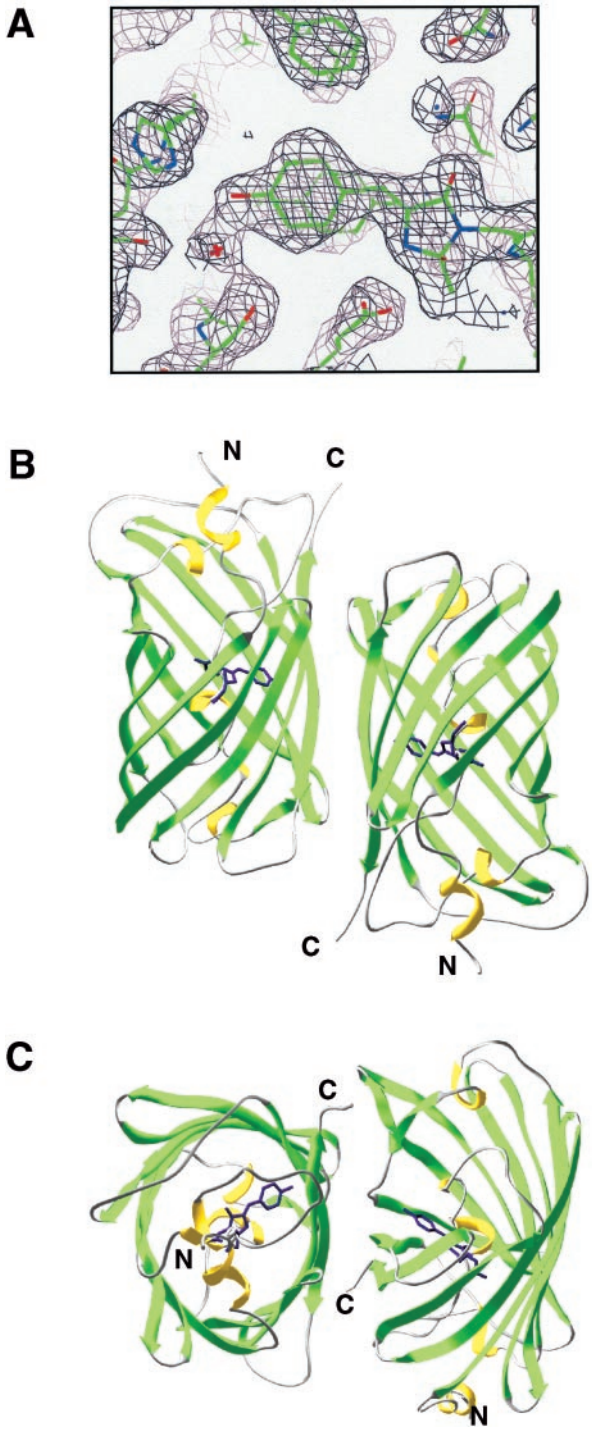


FIG. 1. *A*, $2F_o - F_c$ electron density map contoured by O (17) at 1.5 $\sigma$ showing the refined structure of the chromophore and adjacent residues of Venus. *B* and *C*, *ribbon diagrams* of the Venus dimer at two perpendicular viewing orientations.

and Venus indicates that the dimerization interface differs significantly between the three proteins (Table III). While the residues involved in the dimer interactions are essentially identical between Venus and wtGFP, significant differences are observed between Venus and EYFP. In both Venus and wtGFP, Glu$^{142}$, Tyr$^{145}$, Asn$^{146}$, Asn$^{149}$, Arg$^{168}$, Asn$^{170}$, Glu$^{172}$, Tyr$^{200}$, and Ser$^{202}$ lie within the buried surface between the two subunits, whereas the same EYFP residues are solvent-accessible (Fig. 2*B*). These differences leave Venus with 5% more buried surface area relative to EYFP. In addition, the average intersubunit distance between atoms located within

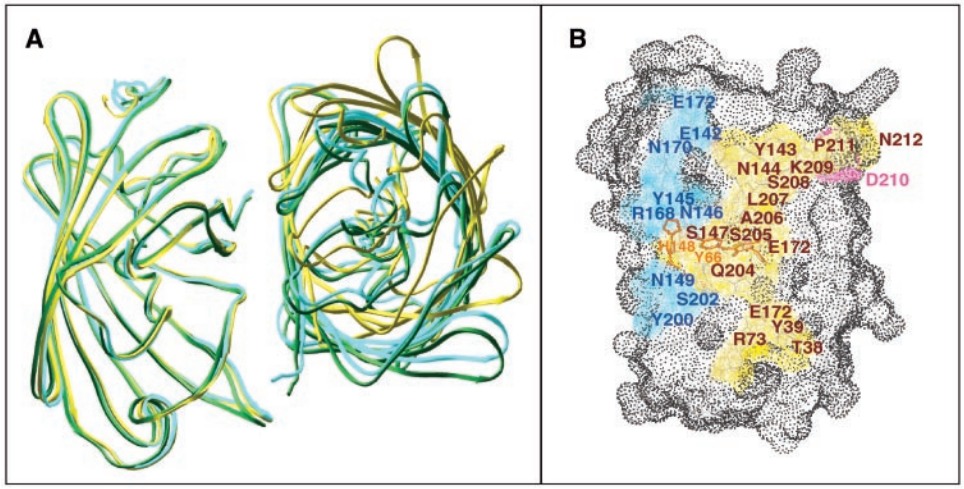


FIG. 2. *A*, *ribbon diagram* showing relative comparison of Venus (*cyan*), EYFP (*yellow*), and wtGFP (*green*) dimer orientations. α-Carbons of residues 5–60 and 70–225 from one monomer of each protein are superimposed. *B*, surface diagram generated by Insight II, showing differences in dimer interfaces of EYFP and Venus. *Yellow*, residues forming dimer contacts both in EYFP and Venus; *cyan*, residues forming dimer contacts only in Venus; *pink*, residues forming dimer contacts only in EYFP. The positions of the chromophore and $His^{148}$ are indicated in *orange*.

TABLE III
*Comparison of selected geometrical parameters in the structures of Venus, EYFP, and wtGFP*

| | Buried surface area per molecule[a] | Distance between monomers[b] | Tilt angles between monomers[c] | | | Shortest diameter of the β-barrel[d] |
|---|---|---|---|---|---|---|
| | | | α | β | γ | |
| | *Å²* | | | | | |
| Venus | 803.43 | 4.27 ± 0.54 | 179.9 | 120.0 | 0.1 | 21.93 ± 1.6 |
| EYFP | 765.83 | 4.40 ± 0.47 | 173.7 | 112.3 | 7.1 | 22.33 ± 1.6 |
| wtGFP | 823.60 | 4.31 ± 0.52 | 178.8 | 120.6 | 0.6 | 22.10 ± 1.7 |

[a] Buried surface area was calculated using CNS (16) with probe radius 1.4 Å.
[b] Distance between monomers was obtained as a mean of distances between chemical groups belonging to different monomers in the buried surface (obtained from MOLMOL (23)) with a limit of 5 Å (±S.D.).
[c] Angles α, β, and γ described in terms of rotation of one monomer relative to the other around *x*, *y*, and *z* axes. The *z* axis is parallel to the long axis of the "reference" monomer; the *y* axis is perpendicular the long axes of both monomers. The angles were measured using program ROTMAT from the CCP4 package (25).
[d] The shortest diameter of the barrel was determined using distances between Cα atoms belonging to residue pairs Y106 and L207, K107 and A206, T108 and S205, and R109 and Q204.

the buried surface of the Venus dimer is somewhat shorter than that of EYFP (Table III). These concurring results indicate that Venus has a larger dimerization interface than EYFP.

Wachter *et al*. (10, 18) have shown that the fluorescence intensity of YFP is inversely related to the concentration of halide ions in solution. This group identified a halide-binding site proximal to the EYFP-H148Q chromophore, which suppresses chromophore fluorescence upon ion binding. The halide-binding cavity is adjacent to the backbone carbonyl groups of $Tyr^{66}$ and $Gly^{67}$ (Fig. 4*B*). Two mutations (T203Y and V68L) located at the buried halide ion-binding cavity of EYFP (Fig. 4*B*) have been implicated in halide sensitivity (18). The halide ion sensitivity of YFPs has led to their use as halide ion sensors (13). Despite the presence of these mutations in Venus, no halide sensitivity has been observed.

The introduction of H148Q into EYFP enhances the halide affinity due to a better access of the ion to its binding cavity via a solvent channel, formed at a β-bulge located close to the dimer interface (10, 18). Venus has a cavity essentially identical to that of EYFP-H148Q in both size and side chain configuration. However, analogous mutagenesis performed on Venus led to no changes in halide affinity.[2] Supported by structural information available on Venus, these data indicate that the β-bulge is inaccessible to halide ions due to rearrangement of the intersubunit interface. This rearrangement centered at the β-bulge is most likely initiated by F64L, a mutation that induces a relocation of many β-strand residues at the dimer interface.

Consistent with the aforementioned observation on the Venus β-bulge, the wtGFP β-bulge is also inaccessible to halide ions (7). The β-bulge residues $Tyr^{145}$, $Asn^{149}$, and $Arg^{168}$ participate in dimer contacts in both Venus and wtGFP, while the same residues are fully solvent exposed in EYFP (Fig. 2*B*). These results suggest that the intersubunit interface could influence the chromophore environment, linking the dimerization mechanism to the fluorescence property of GFP and its variants (8).

### *Venus-specific Mutations*

As stated previously, Venus contains five additional mutation sites relative to EYFP (Table I). Comparison of the corresponding crystal structures helped explain the effects of these mutations on Venus properties. M153T, V163A, and S175G were found to improve the rate of maturation, while mutations F46L and F64L induced a number of local and global structural changes. Here we describe the individual effect of each mutation in detail.

*F46L*—In the EYFP structure, the $Phe^{46}$ phenyl ring exhibits an antiparallel π-π stacking to the phenyl ring of $Phe^{64}$ (Fig. 4*A*). Substitution of each aromatic side chain with an alkyl side chain creates a vacancy at residue 46. This change in side chain orientation results in close hydrophobic contact between residue $Leu^{46}$ and the neighboring residue $Leu^{44}$ as well as an associated change in the $Leu^{42}$ side chain. The F46L mutation

[2] T. Nagai and A. Miyawaki, unpublished data.

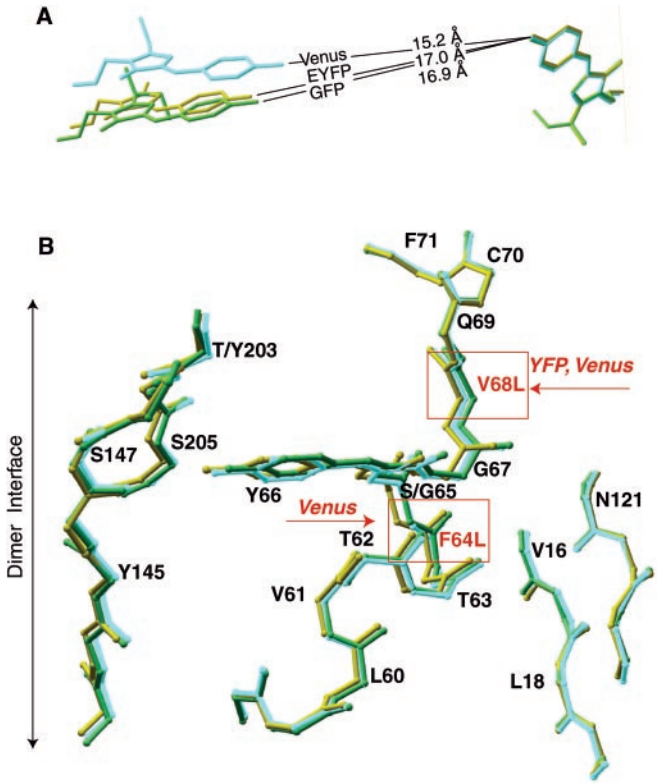


FIG. 3. *A*, view of chromophore pairs belonging to Venus (*cyan*), EYFP (*yellow*), and wtGFP (*green*) dimers, showing distances between phenol oxygens, produced by MOLMOL (23). *B*, *ball and stick diagram* showing the effect of F64L (Venus) and V68L (EYFP and Venus) mutations on the position of the chromophore and the central helix within the protein molecule. Backbone representation of the chromophore area in Venus (*cyan*), EYFP (*yellow*), and wtGFP (*green*) is shown.

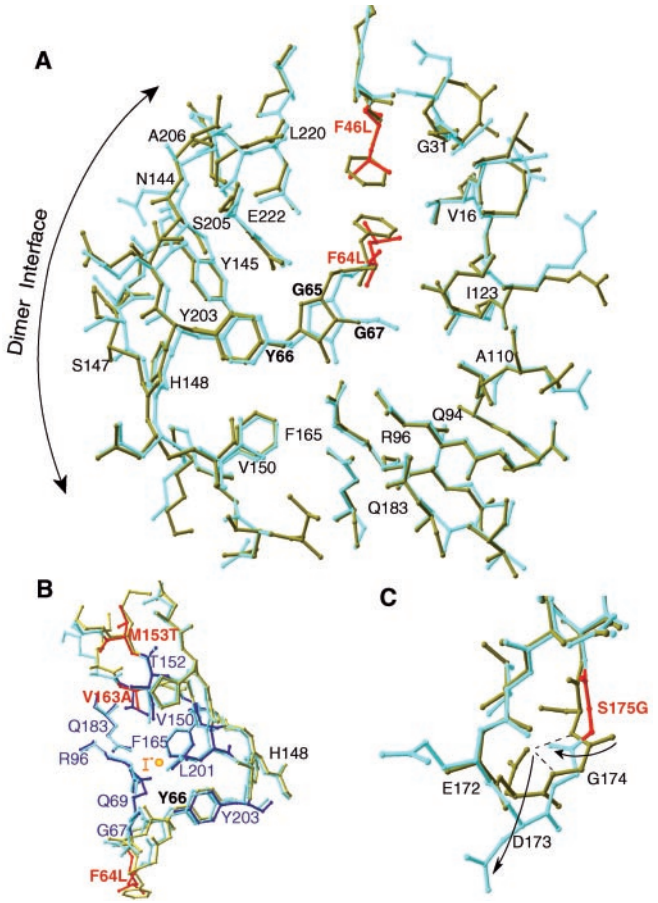


FIG. 4. **Diagrams illustrating structural differences around mutation sites in Venus (*cyan*) relative to EYFP (*yellow*).** Mutated residues are *red* and colored only in the Venus structure. *A*, F46L and F64L, the cross-section view of the β-barrel showing both mutated residues (*red*), the chromophore and adjacent residues, as well as the relocation of β-strands in Venus relative to EYFP, forming the dimer interface. *B*, M153T, V163A, and F64L. The iodide-binding site of EYFP is shown in *orange* and residues forming this binding site in *blue*. Structures superimposed are Venus and EYFP (Protein Data Bank code 1YFP). The position of the iodide ion was taken from Protein Data Bank code 1F09 (18). *C*, S175G. Differences in the position of $Asp^{173}$ side chain and the carbonyl of $Gly^{174}$ (depicted by *arrows*), initiated by the S175G substitution, result in a more relaxed conformation of the loop in Venus relative to EYFP. Possible hydrogen bonds in EYFP are shown as *dashed lines*.

was found to improve maturation at 37 °C (15) by removing steric and energetic constraints, which may hinder folding of the polypeptide chain (Table I). Furthermore, the Venus F46L substitution accelerates the oxidation of the Cα–Cβ bond of $Tyr^{66}$ during chromophore formation (15). Interestingly, major functional changes caused by the F46L mutation resemble those seen in GFP-S65T (6, 21) and DsRed N42H/Q (22), which show an increased rate of oxidation relative to their "precursor" proteins, wtGFP and wild-type DsRed, respectively. In GFP-S65T, the introduction of the threonine side chain at chromophore position 65 repositions the $Leu^{44}$ and $Leu^{42}$ side chain. In DsRed-N42H/Q, the more bulky side chain of $His^{42}$ or $Gln^{42}$ shifts toward a position similar to $Leu^{42}$ in Venus, leading to a repositioning of $Gln^{66}$, an equivalent to residue 65 in Venus and EYFP. In brief, the introduction of F46L causes a series of changes at residues 42, 44, and 65, facilitating an increased rate of maturation. In addition, a change concerning residue 65 (66 in DsRed) in the Venus chromophore may lead to an increased rate of oxidation.

*F64L*—In EYFP, the V68L substitution reorients both the central helix and the chromophore toward the protein surface (8). In Venus, however, the substitution of phenylalanine with leucine at position 64 counteracts any change in orientation caused by V68L, and the central helix and the chromophore remain roughly in their wild-type positions. Therefore, when compared with EYFP, the Venus chromophore is shifted ~0.5 Å toward the center of the molecule (Figs. 3*B* and 4*A*). A similar dislocation of neighboring residues $Tyr^{145}$, $Tyr^{203}$, $Leu^{220}$, and $Glu^{222}$ accompanies this slight movement of the central helix. Such structural changes also influence the position of β-barrel strands G, J, and K as well as part of strand H. The shifted β-strands contain residues involved in the dimer interface, such as N144, S147, and A206 (Fig. 4*A*). Relocation of these residues causes a small decrease in the average diameter of the β-barrel and geometric "flattening" of the β-barrel itself, increasing the surface area buried between the two monomers relative to EYFP. The β-strand movement occurs in close parallel to the movement of the chromophore and the central helix, and hence the distances between the residues surrounding the chromophore remain essentially unchanged in Venus relative to EYFP. The implications of the F64L mutation may therefore involve a reduction in halide ion binding to Venus (as discussed above under "Dimeric Structure and Halide Sensitivity").

*M153T and V163A*—Both $Thr^{153}$ and $Ala^{163}$, commonly mutated to improve protein maturation, are located in the loop region between strands G and H. This region is situated in close proximity to the halide-binding site but away from the dimer interface in the EYFP (Fig. 4*B*). There is no obvious difference in the orientation of side chains of residues 153 and 163 between Venus and EYFP, where the polar side chain of $Thr^{153}$ remains exposed to the solvent, and the side chain of $Ala^{163}$ continues to point toward the molecular interior. Based

on its location near to the halide-binding site, the V163A mutation may also be involved in eliminating chloride sensitivity in Venus (18) (Fig. 4*B*).

*S175G*—The S175G mutation is located in a short turn between strands H and I. The removal of the hydroxyl group of serine drastically alters the backbone conformation of the region spanning residues 173–175. Such a change involves breaking the three-centered hydrogen bond found in EYFP between the side chain carboxyl oxygen atom of $Asp^{173}$ and the amide nitrogens of $Gly^{174}$ and $Ser^{175}$. This is caused by ~180° rotation of the carboxyl side chain of $Asp^{173}$, which flips away from the backbone carbonyl of $Gly^{174}$, resulting in its complete exposure to the solvent (Fig. 4*C*). The S175G mutation in cycle-3 GFP (5) and Venus (15) has been shown to facilitate the protein folding process *in vivo*. S175G also enhances the fluorescence intensity of ECFP 2-fold in an *in vitro* experiment.[2] While the exact structural basis of this increased folding rate is unclear, it should be noted that a localized conformational change outside of the β-barrel (Fig. 4*C*) significantly impacts the properties of the chromophore within the β-barrel, including maturation.

*Concluding Remarks*—The five mutations that distinguish Venus from EYFP increase the rate of maturation and abolish the sensitivity to halide ions (15). The 2.2-Å x-ray structure of Venus reveals several structural differences when compared with EYFP and wtGFP, thus helping to elucidate the structure-function relationship of this fluorescent protein. Among the five mutations, those known as "folding mutations" (4, 15) seem to facilitate the maturation process by introducing highly flexible, smaller side chains within the loop regions located outside the β-barrel (M153T, V163A, S175G) or near the chromophore (F64L). The F46L mutation promotes a local structural change near the chromophore, which consequently accelerates oxidation, a rate-limiting step in chromophore maturation. In addition, we found that the F64L mutation is responsible for a major structural change inside the β-barrel, leading to an alteration of the intersubunit orientation, ultimately preventing halide ion access to the binding cavity near the chromophore.

Two properties of Venus, however, remain to be explained, including the small red shift of the absorption peak attributed to a neutral chromophore and the increased resistance to low pH when compared with EYFP. This observed small red shift might be attributed to the fact that the aromatic rings of the Venus chromophore and $Tyr^{203}$ have a more parallel orientation, minimizing the energy interaction. Alternatively, the pH resistance may result from the slightly smaller distance between $His^{148}$ and the chromophore, thus stabilizing the associated hydrogen bond and promoting the ionic chromophore form. As both properties are pH-dependent, a comparison of the present structure at pH 8.4, with a Venus structure obtained at lower pH is needed to address these questions.

*Acknowledgments*—We thank Kit Tong and Jane Gooding for assistance.

REFERENCES

1. Prasher, D. C., Eckenrode, V. K., Ward, W. W., Prendergast, F. G., and Cormier, M. J. (1992) *Gene (Amst.)* **111,** 229–233
2. Tsien, R., and Prasher, D. (2000) in *Green Fluorescent Protein* (Chalfie, M., and Kain, S., eds) pp. 97–118, Wiley-Liss, New York
3. Heim, R., Prasher, D. C., and Tsien, R. Y. (1994) *Proc. Natl. Acad. Sci. U. S. A.* **91,** 12501–12504
4. Yokoe, M., and Meyer, T. (1996) *Nat. Biotechnol.* **14,** 1252–1256
5. Bastianutta, R., Negro, A., and Zanotti, G. (2000) *Proteins* **41,** 429–437
6. Ormö, M., Cubitt, A. B., Kallio, K., Gross, L. A., and Tsien, R. Y. (1996) *Science* **273,** 1392–1395
7. Yang, F., Moss, L. G., and Phillips, G. N. J. (1996) *Nat. Biotechnol.* **14,** 1246–1251
8. Ward, W. W. (1998) in *Green Fluorescent Protein* (Chalfie, M., and Kain, S., eds) pp. 45–75, Wiley & Sons Inc., New York
9. Phillips, G. N. J. (1997) *Curr. Opin. Struct. Biol.* **7,** 821–827
10. Wachter, R. M., Elsliger, M.-A., Kallio, K., Hanson, G. T., and Remington, S. J. (1998) *Structure (Lond.)* **6,** 1267–1277
11. Wachter, R. M., and Remington, S. J. (1999) *Curr. Biol.* **9,** R628–R629
12. Takahashi, A., Zhang, Y., Centonze, E., and Herman, B. (2001) *BioTechniques* **30,** 804–812
13. Jayaraman, S., Haggie, P., Wachter, R. M., Remington, S. J., and Verkman, A. S. (2000) *J. Biol. Chem.* **275,** 6047–6050
14. Griesbeck, O., Baird, G. S., Campbell, R. E., Zacharias, D. A., and Tsien, R. Y. (2001) *J. Biol. Chem.* **276,** 29188–29194
15. Nagai, T., Ibata, K., Park, E. S., Kubota, M., Mikoshiba, K., and Miyawaki, A. (2002) *Nat. Biotechnol.* **20,** 87–90
16. Brünger, A. T., Adams, P. D., Clore, G. M., DeLano, W. L., Gros, P., Grosse-Kunstleve, R. W., Jiang, J. S., Kuszewski, J., Nilges, M., Pannu, N. S., Read, R. J., Rice, L. M., Simonson, T., and Warren, G. L. (1998) *Acta Crystallogr. Sect. D Biol. Crystallogr.* **54,** 905–921
17. Jones, T. A., Zou, J.-Y., Cowan, S. W., and Kjelgaard, M. (1991) *Acta Crystallog. Sect A* **47,** 110–119
18. Wachter, R. M., Yarbrough, D. Y., Kallio, K., and Tsien, R. Y. (2000) *J. Mol. Biol.* **301,** 157–171
19. Yarbrough, D., Wachter, R. M., Kallio, K., Matz, M. V., and Remington, S. J. (2001) *Proc. Natl. Acad. Sci. U. S. A.* **98,** 462-
20. Elsliger, M.-A., Wachter, R. M., Hanson, G. T., Kallio, K., and Remington, S. J. (1999) *Biochemistry* **38,** 5296–5301
21. Heim, R., Cubitt, A. B., and Tsien, R. Y. (1995) *Nature* **373,** 663–664
22. Bevis, B. J., and Glick, B. S. (2002) *Nat. Biotechnol.* **20,** 83–87
23. Koradi, R., Billeter, M., and Wüthrich, K. (1996) *J. Mol. Graphics* **14,** 51–55
24. Reid, B. G., and Flynn, G. C. (1997) *Biochemistry* **36,** 6786–6791
25. Collaborative Computational Project No. 4 (1994) *Acta Crystallogr. Sect. D Biol. Crystallogr.* **50,** 760–763